Passive Mechanical Properties of Cardiac and Arterial Tissue: A Paired Comparison Study in a Calf Model

Ola Alsaadi[1], Jieyang Zhang[2], Masod Sadipour[2], Ali N. Azadani[2]
[1]Student Contributor, University of Denver
[2]Advisor, Department of Mechanical and Materials Engineering, University of Denver

Abstract

Purpose: The mechanical behavior of heart tissue plays a crucial role in elucidating cardiac physiology and pathophysiology. Accurate measurement of the mechanical properties of cardiac and arterial tissues is indispensable for advancing computer simulations and developing medical devices. This study aimed to assess the passive mechanical properties of cardiac and arterial tissue in a calf model using a paired comparison method.
Methods: A planar biaxial stretching device was used to determine the mechanical characteristics of 84 square specimens obtained from 14 different anatomical regions. Cauchy stress-Green strain curves were constructed for each anatomical area, and a Fung-type constitutive model was applied to fit the raw data. The strain energy and anisotropy index were subsequently calculated.
Results: The experimental results indicated that all tissue specimens exhibited nonlinear responses to biaxial stress. Comparison based on the magnitude of the strain energy function revealed that the aorta showed the highest strain energy, followed by the left ventricles, pulmonary artery, right ventricle, left atrium, and right atrium, respectively. Among the different areas, the left ventricle displayed the highest level of tissue anisotropy. These observations align with previous investigations on human heart tissue.
Conclusion: We comprehensively characterized the mechanical behavior of various heart chambers and significant arteries using rigorous quantitative analysis. The outcomes of this research provide valuable insights for advancing our understanding of heart physiology and exploring potential therapeutic approaches for cardiovascular diseases.

Keywords: *Passive Mechanical Properties, Planar Biaxial Testing, Cardiac and Arterial Tissue, Anisotropy*

LIST OF ABBREVIATIONS

LVA: Left ventricle anterior
LVP: Left ventricle posterior
LVL: Left ventricle lateral
LVS: Left ventricle septal
RVA: Right ventricle anterior
RVP: Right ventricle posterior
LAA: Left atrium anterior
LAP: Left atrium posterior
RAA: Right atrium anterior
RAP: Right atrium posterior
AA: Aorta anterior
AP: Aorta posterior
PAA: Pulmonary artery anterior
PAP: Pulmonary artery posterior

1 INTRODUCTION

Understanding how heart and artery tissues respond to force is crucial for comprehending their normal function

within physiological contexts. Changes in soft tissue mechanical properties, which are demonstrated by how tissues handle loading, can contribute to cardiovascular diseases. Investigating these mechanical properties is essential for developing effective treatments and interventions. Biological tissues exhibit complex mechanical behavior, necessitating the consideration of various structural responses, such as nonlinear stress-strain relationships, mechanical anisotropy (the directional dependence of mechanical properties within soft tissues), and viscoelasticity (time-dependent mechanical properties displaying both viscous and elastic behavior)[1]. It is essential to develop robust constitutive models to accurately model and understand these tissues for physiological, diagnostic, and therapeutic applications. Early investigations primarily relied on uniaxial tensile tests[2;3]; however, due to the mechanical anisotropy of cardiac and arterial tissues, uniaxial data is inadequate for parameter estimation of three-dimensional constitutive models as it focuses solely on one direction. Soft tissues, in general, exhibit anisotropic mechanical behavior, which varies in three dimensions based on the tissue's location in the body. Biaxial tests have been used successfully for parameter estimation of nearly incompressible materials, including biological tissue, where thin sections can be obtained or prepared[4;5;6;7]. In addition, triaxial testing systems have been employed to investigate the mechanical properties of biological tissue under a multi-axial stress state[8;9;10]. The triaxial tests can provide a comprehensive data set for the characterization of thick-walled organs. However, the availability of triaxial equipment is limited, and the mounting of tissue is challenging. These advanced testing methodologies offer superior physiological relevance and provide crucial direction-dependent mechanical information about the tested specimens.

The mechanical properties of cardiac and arterial tissues are essential for their proper functioning and are intimately linked to various pathophysiological conditions (e.g., heart failure, aortic aneurysm, aortic dissection, etc.). Despite their identical embryonic origin, the mechanical properties of cardiac and arterial tissue undergo dynamic changes throughout growth and adulthood. Prior studies have primarily examined specific anatomical regions, necessitating additional research to comprehensively characterize the mechanical properties of all heart chambers and major arteries using a paired-matched analysis. This comprehensive understanding of mechanical behavior has significant implications for designing innovative medical devices and assessing treatment modalities for cardiovascular diseases. In this study, we employed a calf model to quantitatively assess the passive mechanical properties (i.e., response to mechanical forces without active muscle activation) of cardiac and arterial tissue. The calf model was chosen due to its similarity to the human heart regarding functional characteristics and established use in device-related investigations, such as left ventricular assist devices[11]. Our goal was to comprehensively characterize the mechanical behavior of various heart chambers and significant arteries using quantitative analysis.

2 MATERIALS AND METHOD

2.1 Biaxial Testing Sample Preparation

Six fresh healthy calf hearts were purchased from a nearby slaughterhouse on harvest morning and frozen at -20°C for later analysis. The hearts were thawed in a 37°C water bath before testing. The left and right ventricles were cut open, and thin slices were obtained from the middle layer of the ventricular free wall using a commercial meat slicer (Chef'sChoice Model 632 Gourmet Electric VariTilt Food Slicer, Avondale, PA, USA). Square specimens were excised from six anatomical regions:

1. Left ventricle anterior (LVA), posterior (LVP), septal (LVS), and lateral (LVL),
2. Right ventricle anterior (RVA) and posterior (RVP),
3. Left atrium anterior (LAA) and posterior (LAP),
4. Right atrium anterior (RAA) and posterior (RAP),
5. Aorta anterior (AA) and posterior (AP),
6. Pulmonary artery anterior (PAA) and posterior (PAP).

Samples from the heart chambers were cut so that the edges were parallel and perpendicular to the predominant fiber direction as judged by the eye. Samples from the aorta and pulmonary arteries were cut so that the edges were parallel and perpendicular to the circumferential direction of the arteries. By testing in both the fiber and cross-fiber directions, we can gain a comprehensive understanding of the tissue's anisotropic mechanical behavior under different loading conditions. A digital caliper (Mitutoyo Model 500-754-10, Aurora, IL, USA) measured sample thickness and length. Following the measurements, the specimens were stored in a phosphate-buffered normal saline solution (Research Products International, Mount Prospect, IL, USA) at 37°C.

2.2 Biaxial Testing System

The mechanical characteristics of the specimens were assessed using a two-dimensional (planar) biaxial test system (CellScale BioTester, Waterloo, ON, Canada). The steps involved in the biaxial testing protocol have already been described by Javani et al.[7]. Briefly, the samples were mounted on the CellScale BioTester equipped with four high-performance actuators to move the arms, along with two inline load cells (Honeywell Load Cells

Model 31, Columbus, OH, USA). To mimic physiological conditions, the samples were completely immersed in a normal saline bath at 37°C. Graphite powder was also added to the top surface of tissue samples to track tissue deformation with a camera mounted on the top at a rate of 15 Hz. The load cells were zeroed before loading started. Then, the specimens underwent ten cycles of 10% equi-biaxial strain at 0.5 Hz as a preconditioning procedure. Subsequently, each sample underwent an equi-biaxial strain of up to 50% with a 4 s stretch and a 4 s recovery duration. After the biaxial testing, the deformation of the specimens was obtained using CellScale LabJoy image tracking software.

2.3 Constitutive Modeling

The specimens were assumed to be incompressible because soft tissue is mostly composed of water[12]. Cauchy stresses (T_{11}, T_{22}) in the fiber and cross-fiber directions were calculated from planar forces (F_{11}, F_{22}) obtained by the two load cells. Cauchy stress represents the force per unit area acting on a surface within a deformable body.

$$T_{11} = \lambda_1 \frac{F_{11}}{t_0 l_0}, \quad \text{and} \quad T_{22} = \lambda_2 \frac{F_{22}}{t_0 l_0} \tag{1}$$

where t_0 signifies the tissue the initial thickness and the stretch ratio = $\frac{l}{l_0}$ of the deformed tissue l to the length of the tissue at rest l_0. Using the following equations, elements of the green strain tensor (E) were determined:

$$E_{11} = \frac{1}{2}(\lambda_1^2 - 1) \quad \text{and} \quad E_{22} = \frac{1}{2}(\lambda_2^2 - 1) \tag{2}$$

Green strain is a measure of deformation in the material. The stress-strain data were fitted using a four-parameter Fung exponential strain energy function[13].

$$W = \frac{C}{2}(e^Q - 1), \quad Q = c_{11}E_{11}^2 + 2c_{12}E_{11}E_{22} + c_{22}E_{22}^2 \tag{3}$$

E_{11} and E_{22} signify the green strains in the x and y directions, correspondingly. Additionally, c_{11}, c_{22}, c_{12}, and C present the material coefficients. The Fung strain energy function is a mathematical model commonly used to describe the hyperelastic behavior of soft biological tissues. Cauchy stresses were found using the following equations:

$$\begin{aligned} T_{11} &= \frac{1}{2}(c_{11}E_{11} + c_{12}E_{22})Cexp(Q) \\ T_{22} &= \frac{1}{2}(c_{12}E_{11} + c_{22}E_{22})Cexp(Q) \end{aligned} \tag{4}$$

A Levenberg-Marquardt least squares algorithm in MATLAB software (Natick, Massachusetts, USA) was used to fit the strain energy function to the experimental data.

Although the arm displacement rates for the circumferential and longitudinal directions were equal, the strain applied to the specimen's center was not exactly equivalent due to the tears in the tissue began to form and spread at the borders where the tungsten wires were fastened. As a result, the following stress-strain correlations in the equi-biaxial strain state were found:

$$\begin{aligned} T_{11}^{equi} &= (2E+1)E(c_{11} + c_{12})Cexp[(c_{11} + c_{22} + 2c_{12})E^2] \\ T_{22}^{equi} &= (2E+1)E(c_{12} + c_{22})Cexp[(c_{11} + c_{22} + 2c_{12})E^2] \end{aligned} \tag{5}$$

where the equi-biaxial condition was indicated by the superscript *equi*. Moreover, tissue anisotropy was calculated using the difference in material coefficients between the two orientations as follows:

$$K = \frac{2|c_{11} - c_{12}|}{(c_{11} + c_{22} + 2c_{12})} \tag{6}$$

2.4 Data Averaging and Statistical Analysis

The proper method for computing the nonlinear material characteristics of biomedical materials is curved averaging instead of coefficient averaging[14]. As a result, Cauchy stresses at evenly spaced intervals of strain were obtained using Equation 5 to create average curves for each anatomical region. All statistical analyses were carried out in IBM-SPSS 2022 software, and all values were reported as mean ± standard deviation (SD). A p-value less than 0.05 was considered significant for these values. The Shapiro-Wilk test was carried out on each model to check normality[15]. A paired-sample t-test was carried out for normally distributed groups. Additionally, a one-way ANOVA followed by a Games Howell post hoc test were used to compare strain energy values among three groups. A non-parametric Wilcoxon test was used for non-normally distributed groups.

3 RESULTS

A planar biaxial stretching device was used to determine the mechanical characteristics of 84 square specimens obtained from 14 anatomical regions. The average length and thickness of the specimens are presented in Table 1a. In addition, the experimental raw data, representing the biaxial stretching of tissue specimens from the aorta and pulmonary artery, are depicted as Cauchy stress–Green strain plots in the circumferential and longitudinal directions in Figure 1. Figure 2 presents the stress–strain response of tissue specimens from the left and right atria in the fiber and cross-fiber directions. Figure 3 also displays the Cauchy stress–Green strain plots obtained from the left and right ventricles in the fiber and cross-fiber directions. In these figures, the y-axis

represents Cauchy stress, which measures the internal forces acting within a material when subjected to external force, while the x-axis represents Green strain, which measures the deformation occurring within a material when subjected to stress. It is important to note that all regions exhibited a nonlinear response to strain during the testing protocol.

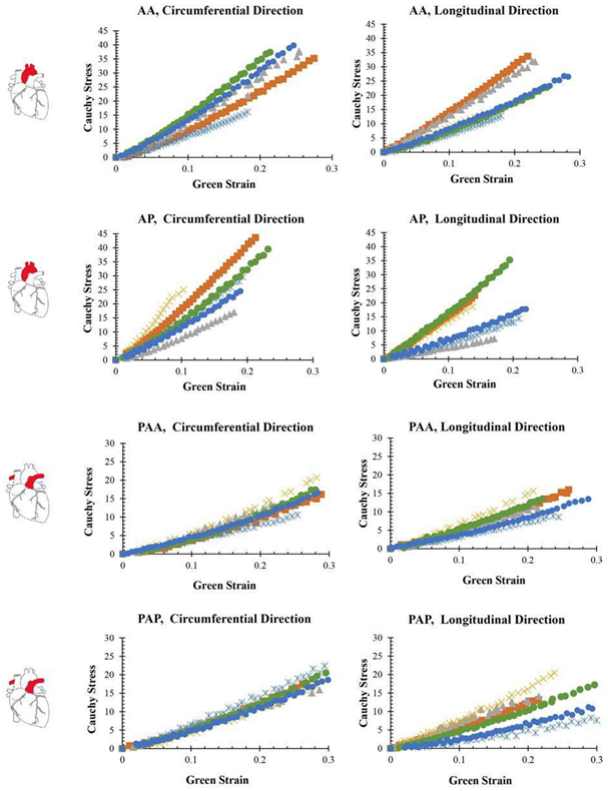

Figure 1. Cauchy stress (KPa)-Green strain data for tissue specimens obtained from anterior and posterior sides of the aorta and pulmonary artery in circumferential and longitudinal fiber directions (six samples represented by distinct colors).

The Fung strain energy function was employed to fit the Cauchy stress-Green strain data for each sample, resulting in the determination of material coefficients. The specific coefficient set for each tissue specimen is provided in the appendix section. Figure 4 illustrates the equibiaxial stress-strain curves for specimens obtained from the anterior and posterior sides of the aorta and pulmonary artery, along with the average curve. Similarly, Figure 5 presents the equibiaxial stress-strain curves and average curves for specimens obtained from the left and right atria. Figures 6 depicts the equibiaxial stress-strain curves and average curve for samples obtained from the left and right ventricles. In these figures, solid lines represent the actual experimental results, while the dashed line corresponds to outliers with stress values exceeding the average stress plus three times the standard deviation.

To quantitatively assess and compare the passive mechanical properties of the anatomical regions, the magnitude of strain energy was calculated for all the specimens at equibiaxial strains of $E_{11} = E_{22} = 0.10$, 0.15, and 0.20. Table 1b presents the mean value and standard deviation of strain energy for each anatomical region. Strain energy refers to the potential energy stored within the specimen when undergoing deformation under applied loads. The comparison between different anatomical regions was conducted in two steps. Firstly, the anterior and posterior portions of all anatomical regions were compared together (for the left ventricles, the lateral and septal sides were also included in the statistical analysis). Secondly, each anatomical region from the left side of the heart was compared with the corresponding region from the right side.

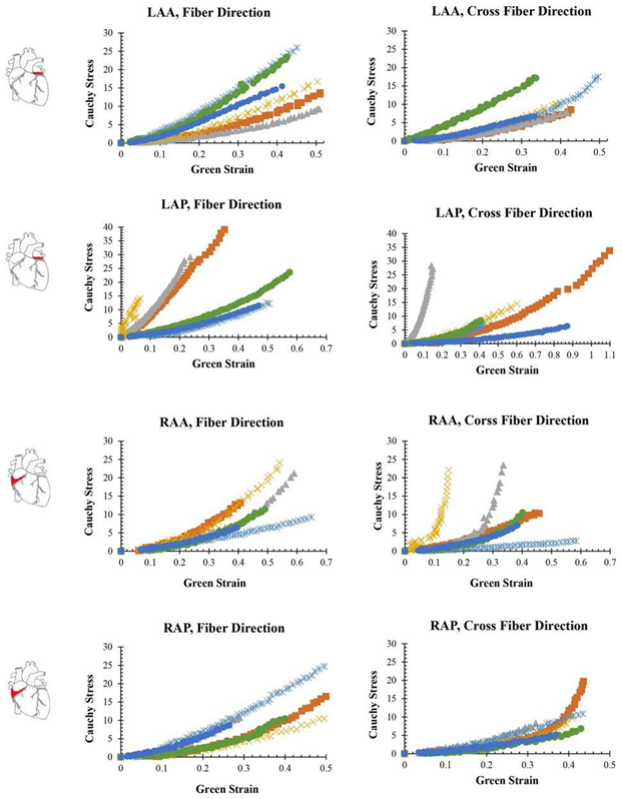

Figure 2. Cauchy stress (KPa)-Green strain data for tissue specimens obtained from anterior and posterior sides of the left and right atria illustrating the effects in fiber and cross fiber directions from both anterior and posterior sides (six samples represented by distinct colors).

Figure 7A summarizes the statistical analysis, presenting the mean and standard deviation of strain energy storage at a strain of 0.15. A one-way ANOVA test was performed to compare the strain energy of different regions of the left ventricles, namely the anterior, posterior, lateral, and septal regions. The analysis indicated no statistically significant difference in strain energy storage between the different portions
(df = 3, Mean Square = 0.089, F = 0.288, Sig. = 0.833). Furthermore, paired sample t-test and Wilcoxon test

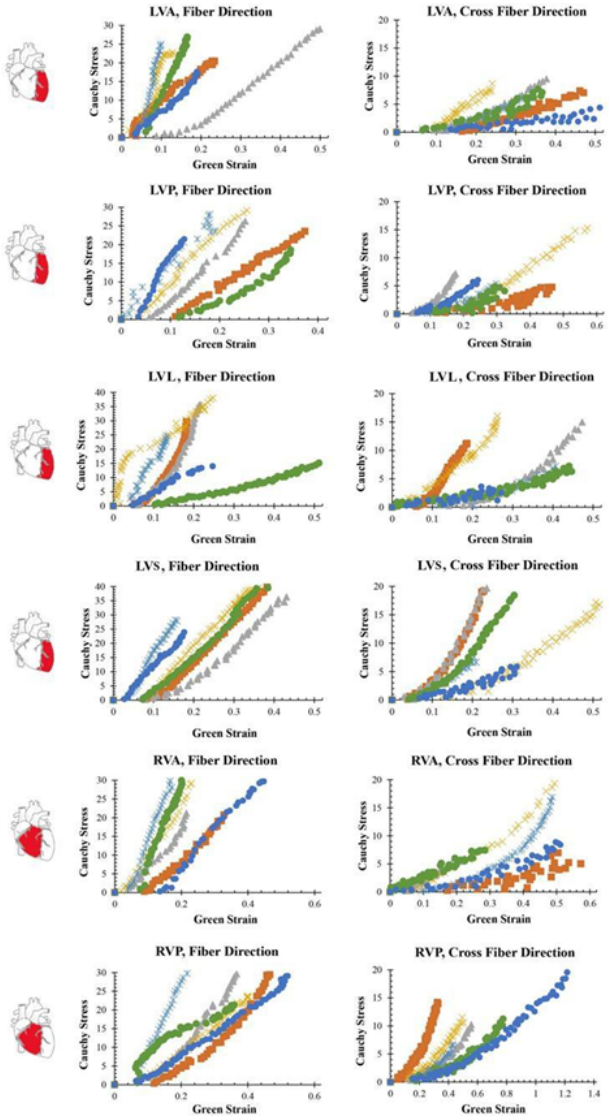

Figure 3. Cauchy stress (KPa)-Green strain data for tissue specimens obtained from the left and right ventricles illustrating the effects in fiber and cross fiber directions (six samples represented by distinct colors).

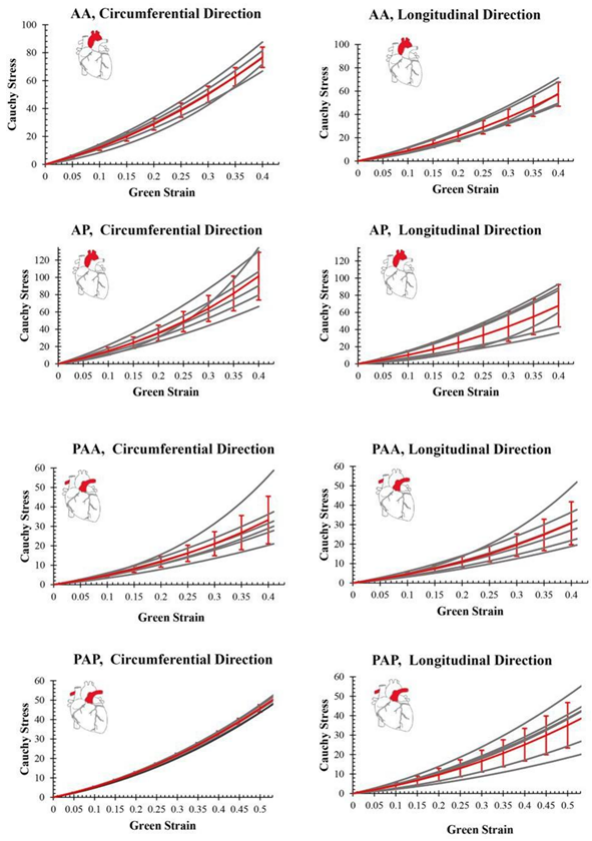

Figure 4. Equibiaxial stress (KPa)-strain curves and the average curve (presented in red) for specimens obtained from the anterior and posterior sides of the aorta and pulmonary artery considering circumferential and longitudinal directions.

were conducted to compare the strain energy storage between the anterior and posterior portions of the left atrium and aorta. The results revealed no statistically significant difference in strain energy storage between the anterior and posterior portions ($p = 0.278$ and $p = 0.345$, respectively). Additionally, a comparison was made between the three anatomical regions on the left side of the heart: the left ventricle, the left atrium, and the aorta. Data from the anterior and posterior portions of the anatomical regions were averaged into one representative dataset for each region (including the lateral and septal sides of the left ventricles). The statistical analysis showed no significant difference in strain energy between the left ventricles and left atria ($p = 0.142$). However, there was a statistically significant difference in strain energy storage between the left atria and the aorta ($p = 0.001$), as well as between the left ventricles and the aorta ($p = 0.014$).

Figure 7B illustrates the statistical comparison between the regions of the right heart. The paired sample t-test and Wilcoxon test results indicated significant differences in strain energy between the anterior and posterior portions of the right ventricles ($p = 0.046$). However, the differences between the anterior and posterior portions of the right atrium and the anterior and posterior portions of the pulmonary artery were not statistically significant ($p = 0.463$ and $p = 0.355$, respectively). Data from the anterior and posterior parts of the anatomical regions were averaged into one representative dataset for each position. The paired sample t-tests were conducted to statistically compare the groups. The results revealed significant differences between the right ventricles and right atrium ($p = 0.017$), significant differences between the right atrium and pulmonary artery ($p < 0.001$), and no significant difference between the right ventricles and pulmonary artery ($p = 0.3$). Furthermore, Figure 7C presents the t-test comparison between the corresponding areas on the left and right sides. The left and right ventricles showed no significant differ-

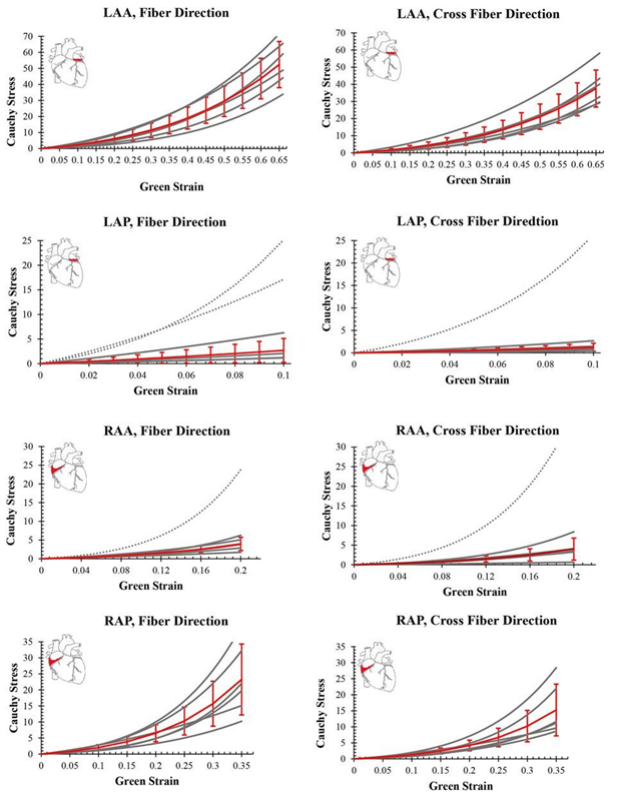

Figure 5. Equibiaxial stress (KPa)-strain curves and the average curve (presented in red) for specimens obtained from the anterior and posterior sides of the left and right atria. with solid lines representing experimental results and dashed lines indicating outliers.

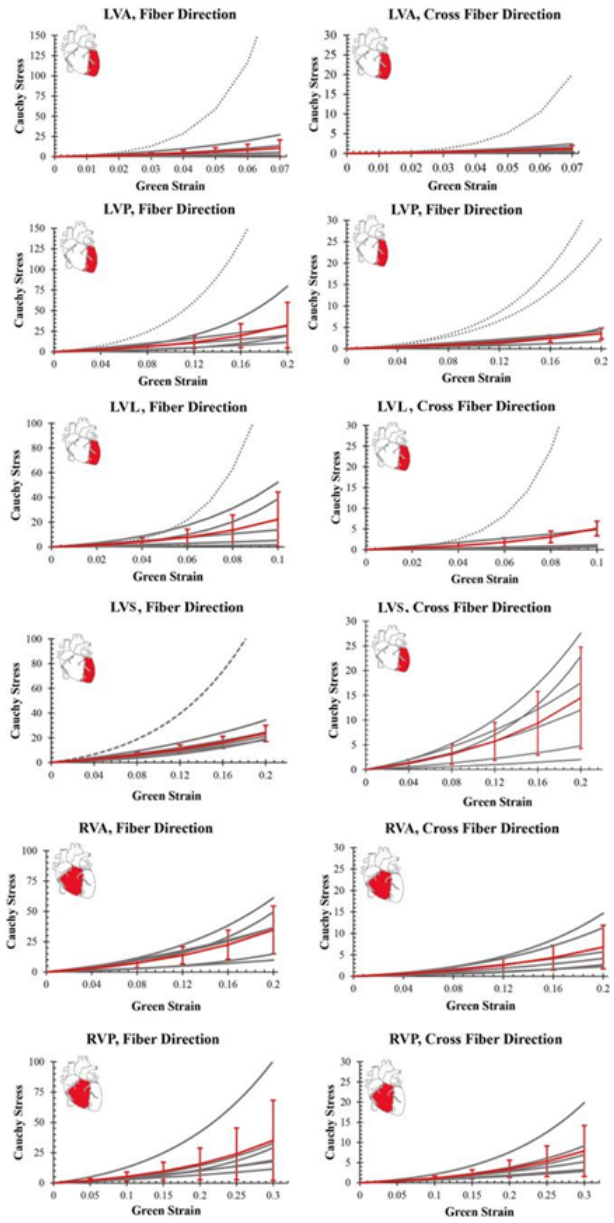

Figure 6. Equibiaxial stress (KPa)-strain curves and the average curve (presented in red) for specimens obtained from the left and right ventricles, distinguishing experimental results (solid lines) from outliers (dashed lines).

ences ($p = 0.068$); however, the left atrium and aorta showed significant differences ($p = 0.046$), and the aorta and pulmonary artery showed significant differences ($p < 0.001$).

Lastly, the anisotropy index (K) was determined using Equation 6 which quantifies the degree of directional dependence of the physical characteristics. This index is particularly relevant for fibrous tissues as they exhibit a certain orientation of tissue fibers that leads to directional certainty in their mechanical characteristics [16]. When the K value is 0, the material has the same properties in all directions, indicating isotropy. A K value greater than 0 indicates some level of anisotropy, with higher values indicating higher anisotropy. Table 1c presents the average and standard deviation of tissue anisotropy for all the anatomical regions. It was observed that the left ventricles had the highest K value ($K = 1.451 \pm 0.289$) while the pulmonary artery had the lowest K value ($K = 0.106 \pm 0.070$). A normality test was conducted for all K values, and paired sample t-tests were used to compare the left regions to their corresponding right regions. The results showed no significant difference in tissue anisotropy between the left and right ventricles, left and right atria, or the aorta and pulmonary artery ($p = 0.878$, $p = 0.249$, and $p = 0.086$, respectively). Furthermore, paired sample t-tests revealed no statistically significant difference in anisotropy between the anterior and posterior portions of different anatomical regions. For the left ventricles, a one-way ANOVA test showed no statistically significant difference in anisotropy between the anterior, posterior, lateral, and septal areas.

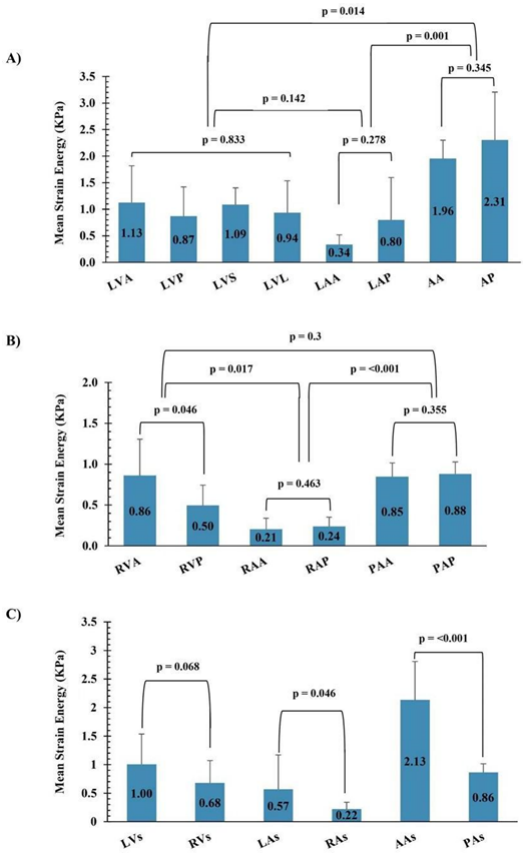

Figure 7. Mean values ± SD of strain energy storage at strain of 0.15 for anatomical regions of the left side (A) and right side (B) of the heart. (C) The results of t-test between corresponding regions from the left and right sides of the heart, with * indicating a non- parametric test and ** signifying one-way ANOVA.

4 DISCUSSION

This study aimed to assess the mechanical properties of various anatomical regions in the calf heart using planar biaxial testing. The experimental data of these regions were fitted to a Fung-type strain energy function. The root mean square (RMS) values of the curve fitting process were found to be low, indicating an excellent fit of experimental data to the model. Subsequently, the material coefficients were utilized to calculate the anisotropy index and then the equibiaxial stress-strain curves. Statistical analysis revealed that the heart's left chambers exhibited significantly higher strain energy than their right counterparts. Other than the anterior and posterior regions of the right ventricle, no statistically significant differences in strain energy storage were observed between the anterior and posterior portions of the same heart regions. The ventricles had higher anisotropy than the other regions, with the left ventricle being the most anisotropic among all.

The mechanical properties of heart tissue show similarities between humans and animals. A study conducted by Sommer et al.[10] aimed to investigate the mechanical properties of various regions within the human myocardium by using biaxial extension tests. The results demonstrated that all tissue specimens exhibited greater stiffness in the fiber direction compared to the cross-fiber direction. Specifically, the stiffness of the human myocardium in the fiber direction was approximately twice as high as that in the cross-fiber direction, as observed on average. In our study, we also observed similar behavior, where tissue in the fiber direction displayed greater stiffness compared to tissue in the cross-fiber direction, except for the anterior region of the right atrium. Comparing different animal models, similar behavior was observed in another study involving animal models. Javani et al.[7] conducted a study to investigate the passive mechanical properties of the sheep heart. Their statistical analysis revealed that the chambers on the left side of the heart exhibited significantly greater stiffness compared to those on the right side. Moreover, the ventricles displayed the highest amount of strain energy storage, while the appendages and atria showed lower levels. This consistent trend was observed on both sides of the heart.

Understanding the impact of age on the mechanical behavior of heart tissue is crucial for developing age-specific interventions and treatments for cardiac conditions[17;18]. In a study conducted by Ahmad et al.[6], the focus was on characterizing the mechanical behavior of neonatal cardiac tissue in porcine models to better understand the differences between neonatal and mature cardiac tissue. Through uniaxial testing, the study revealed that neonatal porcine cardiac tissue was approximately half as stiff as mature tissue and about one-third as stiff in biaxial testing. The authors observed that age-related changes in the cardiac matrix, such as increased collagen fibril cross linking and assembly, contribute to the increased stiffness observed in mature tissue[19]. Therefore, evaluating and comparing the mechanical properties of heart tissue across different age groups is essential for a comprehensive understanding of the influence of age on cardiac tissue mechanics, which implies the need for future investigation. This knowledge can inform targeted interventions and treatments tailored to specific age-related cardiac conditions.

The current study is subject to certain limitations that should be considered. Firstly, the small sample size, involving only 14 regions from six hearts, reduces the statistical power and may underestimate some differences between the study anatomical regions[20]. To address this, future research should aim to utilize larger sample sizes to enhance the statistical analysis power and facilitate more robust comparisons between the cardiac and arterial tissue. Another limitation of the study is that the specimens used were fresh frozen samples, which may influence their mechanical properties. Frozen tissues tend to exhibit increased stiffness and higher anisotropy compared to fresh tissues[21].

Table 1

Region	**RVA**	**RVP**	**LVA**	**LVP**	**LVS**	**LVL**	**AA**
Avg. length ± SD (mm)	15.215 ± 0.698	15.132 ± 0.574	14.864 ± 0.515	15.282 ± 0.641	14.657 ± 0.643	15.654 ± 0.679	14.325 ± 0.619
Region	**AP**	**PAA**	**PAP**	**LAA**	**LAP**	**RAA**	**RAP**
Avg. length ± SD (mm)	14.334 ± 1.086	14.773 ± 0.736	14.638 ± 0.632	14.999 ± 1.518	13.699 ± 1.348	13.969 ± 1.157	13.924 ± 0.832
Region	**RVA**	**RVP**	**LVA**	**LVP**	**LVS**	**LVL**	**AA**
Avg. thickness ± SD (mm)	2.254 ± 0.517	2.053 ± 0.231	2.392 ± 0.261	2.563 ± 0.365	2.690 ± 0.343	2.605 ± 0.255	3.198 ± 0.448
Region	**AP**	**PAA**	**PAP**	**LAA**	**LAP**	**RAA**	**RAP**
Avg. thickness ± SD (mm)	3.043 ± 0.372	3.094 ± 0.422	3.242 ± 0.567	4.160 ± 1.310	4.050 ± 0.772	4.115 ± 0.508	3.954 ± 0.868

(a) Average length and thickness with standard deviation (SD) for the specimens in stress-free condition.

Region	**W 10%**	**W 15%**	**W 20%**
AA	0.869 ± 0.155	1.957 ± 0.344	3.484 ± 0.602
AP	1.024 ± 0.403	2.307 ± 0.902	4.108 ± 1.590
LAA	0.149 ± 0.081	0.338 ± 0.181	0.605 ± 0.322
LAP	0.345 ± 0.337	0.801 ± 0.798	1.491 ± 1.532
LVA	0.441 ± 0.231	1.128 ± 0.691	2.535 ± 2.114
LVP	0.375 ± 0.236	0.870 ± 0.551	1.623 ± 1.048
LVL	0.387 ± 0.265	0.936 ± 0.602	1.882 ± 1.135
LVS	0.473 ± 0.132	1.086 ± 0.317	1.989 ± 0.621
PAA	0.376 ± 0.076	0.847 ± 0.169	1.510 ± 0.301
PAP	0.391 ± 0.066	0.880 ± 0.148	1.566 ± 0.263
RAA	0.089 ± 0.056	0.206 ± 0.134	0.385 ± 0.263
RAP	0.105 ± 0.050	0.240 ± 0.112	0.437 ± 0.199
RVA	0.376 ± 0.196	0.862 ± 0.445	1.575 ± 0.805
RVP	0.218 ± 0.108	0.497 ± 0.248	0.899 ± 0.457

(b) Mean and standard division of the strain energy for different anatomical regions at 0.10, 0.15, and 0.20 strain levels.

Region	**RVA**	**RVP**	**LVA**	**LVP**	**LVS**	**LVL**	**AA**
Avg. ± SD	0.317 ± 0.214	0.418 ± 0.307	0.325 ± 0.218	0.84 ± 0.528	1.451 ± 0.289	1.353 ± 0.212	0.93 ± 0.673
Region	**LVL**	**RAA**	**RAP**	**RVA**	**RVP**	**PAA**	**PAP**
Avg. ± SD	1.277 ± 0.534	0.346 ± 0.299	0.409 ± 0.333	1.359 ± 0.174	1.179 ± 0.434	0.106 ± 0.070	0.33 ± 0.310

(c) Index of tissue anisotropy (K) for different anatomical regions.

Previous studies have indicated that the freeze/thaw process decreases the fibril area[22]. Therefore, caution should be exercised when extrapolating these findings to fresh cardiac tissue samples. This said, it is important to note that these limitations do not invalidate the study's main conclusion, which demonstrated that tissue from the left side of the heart exhibited significantly higher strain energy storage than the corresponding tissue from the right side. Furthermore, the left ventricle displayed the highest level of tissue anisotropy compared to other regions.

5 CONCLUSION

In summary, this study involved conducting planar biaxial stretch tests on tissue samples obtained from various regions of a healthy calf's heart. Cauchy stress–Green strain curves were constructed for each anatomical area, and a Fung-type constitutive model was applied to fit the raw data. The results indicated that all tissue specimens exhibited nonlinear responses to biaxial stress, attributed to the microstructure's reaction and the involvement of fibers as stretching progresses. Among the different areas, the left ventricle displayed the highest level of tissue anisotropy compared to other regions. Additionally, a comparison based on the magnitude of the strain energy function revealed that the aorta exhibited the highest strain energy, followed by the left ventricles, pulmonary artery, right ventricle, left atrium, and right atrium, respectively. Investigating the mechanical properties and composition of cardiac and arterial tissue is crucial for a comprehensive understanding of the cardiac function and for evaluating potential treatments for cardiovascular diseases. Biomechanical variables are vital determinants of cardiac function, both in healthy and diseased hearts[23]. Utilizing mechanical indicators such as tissue stiffness and strain enables medical professionals to identify patients who could benefit from surgical interventions.

6 ACKNOWLEDGEMENTS

Funding: This work was supported by the University of Denver, Grant number: 84993-142235.

Competing Interests: The authors declare that they have no conflict of interest.

Author Contributions: Ola Alsaadi contributed to collection of data, interpretation of data, and writing the manuscript. Jieyang Zhang contributed to collection of data and interpretation of data. Masod Sadipour contributed to writing the manuscript. AA contributed to study design, interpretation of data, funding, and writing the manuscript.

Ethics Approval: The study was granted exemption and did not require ethics approval.

Consent to Participate: Not applicable.

Consent to Publish: Not applicable.

Data Availability Statement: The raw data was provided in the supplementary material.

7 EDITOR'S NOTES

This article was peer-reviewed.

REFERENCES

[1] Sacks, M. S. & Sun, W. Multiaxial mechanical behavior of biological materials. *Annual Review of Biomedical Engineering* **5**, 251–284 (2003).

[2] Mohan, D. & Melvin, J. W. Failure properties of passive human aortic tissue. i—uniaxial tension tests. *Journal of Biomechanics* **15**, 887–902 (1982).

[3] Humphrey, J. D. & Yin, F. C. P. On constitutive relations and finite deformations of passive cardiac tissue: I. a pseudostrain-energy function. *Journal of Biomechanical Engineering* **109**, 298–304 (1987).

[4] Zemánek, M., Bursa, J. & Děták, M. Biaxial tension tests with soft tissues of arterial wall. *Engineering, Medicine* **16** (2008).

[5] Fatemifar, F., Feldman, M. D., Oglesby, M. & Han, H.-C. Comparison of biomechanical properties and microstructure of trabeculae carneae, papillary muscles, and myocardium in the human heart. *Journal of Biomechanical Engineering* **141** (2019).

[6] Ahmad, F. *et al.* Biomechanical properties and microstructure of neonatal porcine ventricles. *Journal of the Mechanical Behavior of Biomedical Materials* **88**, 18–28 (2018).

[7] Javani, S., Gordon, M. & Azadani, A. N. Biomechanical properties and microstructure of heart chambers: A paired comparison study in an ovine model. *Annals of Biomedical Engineering* **44**, 3266–3283 (2016).

[8] Dokos, S., LeGrice, I. J., Smaill, B. H., Kar, J. & Young, A. A. A triaxial-measurement shear-test device for soft biological tissues. *Journal of Biomechanical Engineering* **122**, 471–478 (2000).

[9] Avazmohammadi, R. *et al.* An integrated inverse model-experimental approach to determine soft tissue three-dimensional constitutive parameters: application to post-infarcted myocardium. *Biomechanics and Modeling in Mechanobiology* **17**, 31–53 (2018).

[10] Sommer, G. *et al.* Biomechanical properties and microstructure of human ventricular myocardium. *Acta Biomaterialia* **24**, 172–192 (2015).

[11] Monreal, G. *et al.* Large animal models for left ventricular assist device research and development. *ASAIO Journal* **60**, 2–8 (2014).

[12] Hadjicharalambous, M., Lee, J., Smith, N. P. & Nordsletten, D. A. A displacement-based finite element formulation for incompressible and nearly-

incompressible cardiac mechanics. *Computer Methods in Applied Mechanics and Engineering* **274**, 213–236 (2014).

[13] Fung, Y. C., Fronek, K. & Patitucci, P. Pseudoelasticity of arteries and the choice of its mathematical expression. *American Journal of Physiology-Heart and Circulatory Physiology* **237**, H620–H631 (1979).

[14] Robertson, D. & Cook, D. Unrealistic statistics: How average constitutive coefficients can produce non-physical results. *Journal of the Mechanical Behavior of Biomedical Materials* **40**, 234–239 (2014).

[15] Ghasemi, A. & Zahediasl, S. Normality tests for statistical analysis: A guide for non-statisticians. *International Journal of Endocrinology and Metabolism* **10**, 486–489 (2012).

[16] O'Shea, D. J., Attard, M. M. & Kellermann, D. C. On fibre dispersion in anisotropic soft biological tissues using fourth-order structural tensors. *International Journal of Solids and Structures* **236-237**, 111052 (2022).

[17] Greeley, W. J. A practice of anesthesia for infants and children, 3rd edition. *Anesthesia & Analgesia* **93**, 1629 (2001).

[18] Cox, R. G. Smith's anesthesia for infants and children - eighth edition. *Canadian Journal of Anesthesia/Journal canadien d'anesthésie* **58**, 973–974 (2011).

[19] Lindsey, M. *et al.* Age-dependent changes in myocardial matrix metalloproteinase/tissue inhibitor of metalloproteinase profiles and fibroblast function. *Cardiovascular Research* **66**, 410–419 (2005).

[20] Button, K. S. *et al.* Power failure: why small sample size undermines the reliability of neuroscience. *Nature Reviews Neuroscience* **14**, 365–376 (2013).

[21] Azarnoosh, M. *et al.* A comparative study of mechanical properties of fresh and frozen-thawed porcine intervertebral discs in a bioreactor environment. *Journal of the Mechanical Behavior of Biomedical Materials* **69**, 169–177 (2017).

[22] Matković, A. & Šarolić, A. The effect of freezing and thawing on complex permittivity of bovine tissues. *Sensors* **22**, 9806 (2022).

[23] Voorhees, A. P. & Han, H. *Biomechanics of Cardiac Function*, 1623–1644 (Wiley, 2015).

Appendix A

AA					AP				
Model 1 c_{11}	**Model 1 c_{12}**	**Model 1 c_{22}**	**Model 1 C**	**Model 1 RMS**	**Model 1 c_{11}**	**Model 1 c_{12}**	**Model 1 c_{22}**	**Model 1 C**	**Model 1 RMS**
0.003	0.003	0.004	17476.3	0.528	0.01	-0.001	0.009	16015.87	0.522
Model 2 c_{11}	**Model 2 c_{12}**	**Model 2 c_{22}**	**Model 2 C**	**Model 2 RMS**	**Model 2 c_{11}**	**Model 2 c_{12}**	**Model 2 c_{22}**	**Model 2 C**	**Model 2 RMS**
0.002	0.002	0.002	37350.5	1.2	1.442	0.366	0.439	36.418	0.331
Model 3 c_{11}	**Model 3 c_{12}**	**Model 3 c_{22}**	**Model 3 C**	**Model 3 RMS**	**Model 3 c_{11}**	**Model 3 c_{12}**	**Model 3 c_{22}**	**Model 3 C**	**Model 3 RMS**
0.014	0.006	0.007	5806.91	0.404	0.002	0.001	0.001	75516.96	1.371
Model 4 c_{11}	**Model 4 c_{12}**	**Model 4 c_{22}**	**Model 4 C**	**Model 4 RMS**	**Model 4 c_{11}**	**Model 4 c_{12}**	**Model 4 c_{22}**	**Model 4 C**	**Model 4 RMS**
0.422	0.222	0.3	97.171	0.284	0.016	0.005	0.005	5464.33	0.422
Model 5 c_{11}	**Model 5 c_{12}**	**Model 5 c_{22}**	**Model 5 C**	**Model 5 RMS**	**Model 5 c_{11}**	**Model 5 c_{12}**	**Model 5 c_{22}**	**Model 5 C**	**Model 5 RMS**
0.023	0.007	0.01	4016.01	0.443	0.007	0.005	0.007	11136.02	0.584
Model 6 c_{11}	**Model 6 c_{12}**	**Model 6 c_{22}**	**Model 6 C**	**Model 6 RMS**	**Model 6 c_{11}**	**Model 6 c_{12}**	**Model 6 c_{22}**	**Model 6 C**	**Model 6 RMS**
0.004	0.002	0.002	21799.58	0.545	0.011	0.004	0.006	6690.64	0.585
LAA					**LAP**				
Model 1 c_{11}	**Model 1 c_{12}**	**Model 1 c_{22}**	**Model 1 C**	**Model 1 RMS**	**Model 1 c_{11}**	**Model 1 c_{12}**	**Model 1 c_{22}**	**Model 1 C**	**Model 1 RMS**
0.804	0.187	0.48	9.748	0.45	0.257	0.031	0.037	176.227	1.538
Model 2 c_{11}	**Model 2 c_{12}**	**Model 2 c_{22}**	**Model 2 C**	**Model 2 RMS**	**Model 2 c_{11}**	**Model 2 c_{12}**	**Model 2 c_{22}**	**Model 2 C**	**Model 2 RMS**
0.616	0.3	0.585	7.363	0.243	2.628	2.19	2.831	16.294	0.907
Model 3 c_{11}	**Model 3 c_{12}**	**Model 3 c_{22}**	**Model 3 C**	**Model 3 RMS**	**Model 3 c_{11}**	**Model 3 c_{12}**	**Model 3 c_{22}**	**Model 3 C**	**Model 3 RMS**
0.628	0.315	0.378	13.917	0.455	1.754	0.135	0.162	60.769	1.392
Model 4 c_{11}	**Model 4 c_{12}**	**Model 4 c_{22}**	**Model 4 C**	**Model 4 RMS**	**Model 4 c_{11}**	**Model 4 c_{12}**	**Model 4 c_{22}**	**Model 4 C**	**Model 4 RMS**
0.486	0.159	0.19	39.055	0.77	0.98	0.384	0.46	6.026	0.47
Model 5 c_{11}	**Model 5 c_{12}**	**Model 5 c_{22}**	**Model 5 C**	**Model 5 RMS**	**Model 5 c_{11}**	**Model 5 c_{12}**	**Model 5 c_{22}**	**Model 5 C**	**Model 5 RMS**
0.174	0.118	0.142	102.091	0.594	0.51	0.137	0.164	24.374	0.268
Model 6 c_{11}	**Model 6 c_{12}**	**Model 6 c_{22}**	**Model 6 C**	**Model 6 RMS**	**Model 6 c_{11}**	**Model 6 c_{12}**	**Model 6 c_{22}**	**Model 6 C**	**Model 6 RMS**
0.512	-0.028	0.317	39.583	0.516	0.525	0.082	0.099	15	0.18
LVA					**LVP**				
Model 1 c_{11}	**Model 1 c_{12}**	**Model 1 c_{22}**	**Model 1 C**	**Model 1 RMS**	**Model 1 c_{11}**	**Model 1 c_{12}**	**Model 1 c_{22}**	**Model 1 C**	**Model 1 RMS**
0.002	0.001	0.001	41722.52	1.567	1.553	0.114	0.137	16.903	1.256
Model 2 c_{11}	**Model 2 c_{12}**	**Model 2 c_{22}**	**Model 2 C**	**Model 2 RMS**	**Model 2 c_{11}**	**Model 2 c_{12}**	**Model 2 c_{22}**	**Model 2 C**	**Model 2 RMS**
1.311	0.274	0.329	12.959	1.448	5.95	1.024	1.229	6.442	1.23
Model 3 c_{11}	**Model 3 c_{12}**	**Model 3 c_{22}**	**Model 3 C**	**Model 3 RMS**	**Model 3 c_{11}**	**Model 3 c_{12}**	**Model 3 c_{22}**	**Model 3 C**	**Model 3 RMS**
7.962	0.72	0.864	13.77	2.583	0.002	0.001	0.001	36333.88	1.992
Model 4 c_{11}	**Model 4 c_{12}**	**Model 4 c_{22}**	**Model 4 C**	**Model 4 RMS**	**Model 4 c_{11}**	**Model 4 c_{12}**	**Model 4 c_{22}**	**Model 4 C**	**Model 4 RMS**

42.673	1.804	2.165	2.131	1.723	0.005	0.001	0.001	24116.09	2.304
Model 5 c_{11}	**Model 5 c_{12}**	**Model 5 c_{22}**	**Model 5 C**	**Model 5 RMS**	**Model 5 c_{11}**	**Model 5 c_{12}**	**Model 5 c_{22}**	**Model 5 C**	**Model 5 RMS**
9.573	0.571	0.686	7.624	1.567	6.443	0.812	0.974	1.567	0.737
Model 6 c_{11}	**Model 6 c_{12}**	**Model 6 c_{22}**	**Model 6 C**	**Model 6 RMS**	**Model 6 c_{11}**	**Model 6 c_{12}**	**Model 6 c_{22}**	**Model 6 C**	**Model 6 RMS**
3.474	0.11	0.166	13.898	0.673	9.05	0.621	0.745	11.206	1.664

LVS					**LVL**				
Model 1 c_{11}	**Model 1 c_{12}**	**Model 1 c_{22}**	**Model 1 C**	**Model 1 RMS**	**Model 1 c_{11}**	**Model 1 c_{12}**	**Model 1 c_{22}**	**Model 1 C**	**Model 1 RMS**
0.667	0.397	0.476	48.726	3.803	28.589	-1.573	11.934	1.259	1.006
Model 2 c_{11}	**Model 2 c_{12}**	**Model 2 c_{22}**	**Model 2 C**	**Model 2 RMS**	**Model 2 c_{11}**	**Model 2 c_{12}**	**Model 2 c_{22}**	**Model 2 C**	**Model 2 RMS**
1.973	-0.089	2.813	14.383	2.294	21.789	-2.814	3.376	2.407	1.075
Model 3 c_{11}	**Model 3 c_{12}**	**Model 3 c_{22}**	**Model 3 C**	**Model 3 RMS**	**Model 3 c_{11}**	**Model 3 c_{12}**	**Model 3 c_{22}**	**Model 3 C**	**Model 3 RMS**
1.239	-0.315	0.391	77.348	2.252	0.002	0.001	0.001	87447.44	5.934
Model 4 c_{11}	**Model 4 c_{12}**	**Model 4 c_{22}**	**Model 4 C**	**Model 4 RMS**	**Model 4 c_{11}**	**Model 4 c_{12}**	**Model 4 c_{22}**	**Model 4 C**	**Model 4 RMS**
5.356	0.472	0.566	20.012	1.973	13.569	-0.807	0.968	9.364	1.506
Model 5 c_{11}	**Model 5 c_{12}**	**Model 5 c_{22}**	**Model 5 C**	**Model 5 RMS**	**Model 5 c_{11}**	**Model 5 c_{12}**	**Model 5 c_{22}**	**Model 5 C**	**Model 5 RMS**
0.98	-0.137	0.692	58.703	2.402	0.402	0.115	0.138	24.545	0.538
Model 6 c_{11}	**Model 6 c_{12}**	**Model 6 c_{22}**	**Model 6 C**	**Model 6 RMS**	**Model 6 c_{11}**	**Model 6 c_{12}**	**Model 6 c_{22}**	**Model 6 C**	**Model 6 RMS**
1.331	0.09	0.108	62.418	1.15	0.282	0.031	0.037	134.29	1.029

RAA					**RAP**				
Model 1 c_{11}	**Model 1 c_{12}**	**Model 1 c_{22}**	**Model 1 C**	**Model 1 RMS**	**Model 1 c_{11}**	**Model 1 c_{12}**	**Model 1 c_{22}**	**Model 1 C**	**Model 1 RMS**
0.873	0.512	0.614	7.93	0.625	1.391	1.151	1.381	2.477	0.753
Model 2 c_{11}	**Model 2 c_{12}**	**Model 2 c_{22}**	**Model 2 C**	**Model 2 RMS**	**Model 2 c_{11}**	**Model 2 c_{12}**	**Model 2 c_{22}**	**Model 2 C**	**Model 2 RMS**
1.598	1.332	2.601	1.936	1.08	1.804	0.66	1.091	6.251	0.55
Model 3 c_{11}	**Model 3 c_{12}**	**Model 3 c_{22}**	**Model 3 C**	**Model 3 RMS**	**Model 3 c_{11}**	**Model 3 c_{12}**	**Model 3 c_{22}**	**Model 3 C**	**Model 3 RMS**
1.867	1.556	3.981	4.144	1.258	0.841	0.52	0.624	5.276	0.509
Model 4 c_{11}	**Model 4 c_{12}**	**Model 4 c_{22}**	**Model 4 C**	**Model 4 RMS**	**Model 4 c_{11}**	**Model 4 c_{12}**	**Model 4 c_{22}**	**Model 4 C**	**Model 4 RMS**
0.003	-0.001	0.002	3302.011	0.172	0.298	-0.083	0.219	104.505	0.476
Model 5 c_{11}	**Model 5 c_{12}**	**Model 5 c_{22}**	**Model 5 C**	**Model 5 RMS**	**Model 5 c_{11}**	**Model 5 c_{12}**	**Model 5 c_{22}**	**Model 5 C**	**Model 5 RMS**
1.34	0.95	1.14	2.497	0.429	1.974	0.725	0.869	2.742	0.342
Model 6 c_{11}	**Model 6 c_{12}**	**Model 6 c_{22}**	**Model 6 C**	**Model 6 RMS**	**Model 6 c_{11}**	**Model 6 c_{12}**	**Model 6 c_{22}**	**Model 6 C**	**Model 6 RMS**
1.845	-0.646	2	5.179	0.233	2.588	-0.131	0.981	6.941	0.287

RVA					**RVP**				
Model 1 c_{11}	**Model 1 c_{12}**	**Model 1 c_{22}**	**Model 1 C**	**Model 1 RMS**	**Model 1 c_{11}**	**Model 1 c_{12}**	**Model 1 c_{22}**	**Model 1 C**	**Model 1 RMS**
3.846	0.349	0.419	4.698	1.151	2.426	0.118	1.619	6.604	0.898
Model 2 c_{11}	**Model 2 c_{12}**	**Model 2 c_{22}**	**Model 2 C**	**Model 2 RMS**	**Model 2 c_{11}**	**Model 2 c_{12}**	**Model 2 c_{22}**	**Model 2 C**	**Model 2 RMS**
4.319	0.673	0.808	9.715	0.656	2.167	0.231	0.277	11.954	1.176

Model 3 c_{11}	**Model 3 c_{12}**	**Model 3 c_{22}**	**Model 3 C**	**Model 3 RMS**	**Model 3 c_{11}**	**Model 3 c_{12}**	**Model 3 c_{22}**	**Model 3 C**	**Model 3 RMS**
2.2	-0.292	0.51	44.747	0.882	0.88	-0.145	0.347	40.358	1.031
Model 4 c_{11}	**Model 4 c_{12}**	**Model 4 c_{22}**	**Model 4 C**	**Model 4 RMS**	**Model 4 c_{11}**	**Model 4 c_{12}**	**Model 4 c_{22}**	**Model 4 C**	**Model 4 RMS**
0.877	0.067	0.081	111.408	2.933	2.921	0.126	0.151	25.427	1.834
Model 5 c_{11}	**Model 5 c_{12}**	**Model 5 c_{22}**	**Model 5 C**	**Model 5 RMS**	**Model 5 c_{11}**	**Model 5 c_{12}**	**Model 5 c_{22}**	**Model 5 C**	**Model 5 RMS**
3.575	0.33	0.396	22.152	1.751	0.001	0.001	0.001	36720.27	2.954
Model 6 c_{11}	**Model 6 c_{12}**	**Model 6 c_{22}**	**Model 6 C**	**Model 6 RMS**	**Model 6 c_{11}**	**Model 6 c_{12}**	**Model 6 c_{22}**	**Model 6 C**	**Model 6 RMS**
0.446	0.052	0.062	62.608	2.481	0.026	0.004	0.004	812.597	1.108
PAA					**PAP**				
Model 1 c_{11}	**Model 1 c_{12}**	**Model 1 c_{22}**	**Model 1 C**	**Model 1 RMS**	**Model 1 c_{11}**	**Model 1 c_{12}**	**Model 1 c_{22}**	**Model 1 C**	**Model 1 RMS**
0.077	0.065	0.088	253.288	0.462	0.012	0.007	0.01	2542.296	0.355
Model 2 c_{11}	**Model 2 c_{12}**	**Model 2 c_{22}**	**Model 2 C**	**Model 2 RMS**	**Model 2 c_{11}**	**Model 2 c_{12}**	**Model 2 c_{22}**	**Model 2 C**	**Model 2 RMS**
0.014	0.009	0.011	1927.36	0.437	0.001	0.001	0.001	44113.86	1.512
Model 3 c_{11}	**Model 3 c_{12}**	**Model 3 c_{22}**	**Model 3 C**	**Model 3 RMS**	**Model 3 c_{11}**	**Model 3 c_{12}**	**Model 3 c_{22}**	**Model 3 C**	**Model 3 RMS**
0.012	0.003	0.012	3610.637	0.244	0.013	0.01	0.015	2038.455	0.515
Model 4 c_{11}	**Model 4 c_{12}**	**Model 4 c_{22}**	**Model 4 C**	**Model 4 RMS**	**Model 4 c_{11}**	**Model 4 c_{12}**	**Model 4 c_{22}**	**Model 4 C**	**Model 4 RMS**
0.003	-0.001	0.003	12089.11	0.345	0.003	0.001	0.001	16003.84	0.847
Model 5 c_{11}	**Model 5 c_{12}**	**Model 5 c_{22}**	**Model 5 C**	**Model 5 RMS**	**Model 5 c_{11}**	**Model 5 c_{12}**	**Model 5 c_{22}**	**Model 5 C**	**Model 5 RMS**
0.534	0.358	0.429	44.46	0.391	0.053	0.028	0.037	555.935	0.214
Model 6 c_{11}	**Model 6 c_{12}**	**Model 6 c_{22}**	**Model 6 C**	**Model 6 RMS**	**Model 6 c_{11}**	**Model 6 c_{12}**	**Model 6 c_{22}**	**Model 6 C**	**Model 6 RMS**
0.006	0.004	0.004	4539.257	0.237	0.228	-0.105	0.174	322.249	0.46

Table 2 The individual coefficient sets (C_{11}, C_{12}, C_{22}, and C) of the four parameter Fung exponential constitutive model for all the individual samples (n = 84) with their root mean square (RMS).